IRAQI JOURNAL OF APPLIED PHYSICS
Vol. 22, No. 3, July-September 2026, pp. 513-524

Nabhan A. Hamdoon [1]
Omar A. Mohammed [2]
Ahmed M. Daabo [3*]
Tawfik Badawy [4]

Numerical Analysis of Thermal Strain Resistance of 6061 Aluminum Alloy under Various Plasma Source Parameters

Recently, plasma sources have served an indispensable function across a wide range of applications, particularly in material fabrication and related thermal loading environments. This study investigates the thermomechanical response of 6061 Al alloy under different plasma heat flux conditions. A coupled thermal structural finite element model was developed and analyzed using ANSYS Workbench 2021 R1. The numerical results were validated against published experimental data and showed good agreement with a 4.4% deviation. Across the investigated plasma heat flux range (0.5 to 0.7 MW/m^2), the simulations predict peak Von Mises stress up to about 5.9 MPa and peak normal stress up to about 2.6 MPa, with the highest stresses localized mainly near the specimen corners. The maximum total deformation increases from about 8.6 μm at the lower heat flux to about 12 μm at the maximum heat flux. Thermal strain also increases with the applied heat flux within the adopted model definition. Overall, the predicted stress and deformation levels remain within the elastic response assumed in the material model, supporting the suitability of 6061 Al alloy for the investigated plasma heat loading conditions.

Keywords: Plasma source; 6061 aluminum alloy; Numerical analysis; ANSYS workbench
Received: 9 January 2026; Revised: 25 March 2026; Accepted: 1 April 2026; Published: 1 July 2026

[1] Department of Refining Engineering, College of Petroleum and Mining Engineering, University of Mosul, Mosul, IRAQ
[2] Department of Mechanical Engineering, College of Engineering, University of Mosul, Mosul, IRAQ
[3] Department of Mining Engineering, College of Petroleum and Mining Engineering, University of Mosul, Mosul, IRAQ
[4] Department of Mechanical Engineering, Faculty of Engineering, Computing and the Environment, Kingston University, London SW15 3DW, UK
* Corresponding author email: ahmeddaboo@uomosul.edu.iq

1. Introduction

Plasma based heat sources are widely used in material processing applications such as surface modification, thermal spraying, joining, and other high heat flux operations. In such procedures, the exposed surface can face spatially concentrated thermal loading, producing steep temperature gradients over very short time. These gradients produce thermal strain as well as thermally induced stresses. Consequently, lead to dimensional imprecision, local yielding, distortion, or damage initiation especially within the constrained regions and geometric disjointedness. Based on that, accurately evaluating their temperature and heat fields as well as their associated thermo-mechanical response under plasma heat flux is significant for the design assessment and reliable operation of engineering components [1-3].

There are many previous studies that addressed plasma wall interaction and high heat flux loading in plasma facing materials, particularly in fusion applications, where thermo-mechanical integration is the most important design concern. Such studies show that the applied amount of heat flux, its distribution, and the cooling or support conditions strongly affect the peak temperature and the location of each; the thermal stress and the thermal strain values [2-4]. From the mechanics' view point, the thermal gradients are a direct source of constrained expansion, and their influences of stress strain growth can be understood through recognized thermo-elastic associations [3]. These considerations encourage the utilization of numerical procedures and techniques in order to solve the combined thermal-structural fields under accurate and realistic working conditions.

For lightweight metallic alloys such as 6061 aluminium alloy, the practical question is whether plasma induced thermal loading can generate significant thermal strain, stress concentration, or deformation within the relevant operating range. Although several previous studies on 6061 aluminium alloy have investigated short time heating, ageing, welding thermal cycles, and post heat treatment effects on mechanical properties and microstructure [5-10], these studies do not directly address the case of a prescribed and spatially localised plasma heat flux acting as a surface thermal boundary condition. As a result, they do not fully capture the coupled thermomechanical response associated with plasma driven surface heating. A more focused assessment is therefore needed in which plasma heating is represented explicitly as an imposed heat flux and the resulting temperature, strain, stress, and deformation fields are quantified.

The finite element analysis (FEA) is well suited for this purpose because it enables direct coupling between heat transfer and structural response while accounting

for boundary constraints, thermal gradients, and material properties. In the present work, the plasma effect is represented in the thermal model as a prescribed surface heat flux boundary condition, and the resulting steady state temperature field is transferred into the structural analysis to evaluate thermal strain and stress development. This modelling strategy is consistent with the thermomechanical framework already adopted in the manuscript and is appropriate when the aim is to assess the first order structural consequences of plasma induced heating rather than to resolve the full plasma discharge physics [1,3,11,12].

Unlike conventional thermal loading where the heat input is typically prescribed from a heater or furnace, the present study represents the thermal load as a surface heat flux derived from plasma electron parameters and applied on the exposed surface. The novelty of the work is the explicit link between representative plasma conditions and the imposed boundary heat flux used to evaluate the resulting thermo mechanical response of Al6061. In this context, plasma heating is treated as a surface driven heat input with strong near surface temperature gradients, rather than a uniform bulk heating condition.

Accordingly, this study investigates the thermomechanical response of 6061 aluminium alloy subjected to plasma heat flux. The research question is: how does the applied plasma heat flux level influence the temperature field and the resulting thermal strain, stress, and deformation of a 6061 aluminium alloy specimen under the investigated conditions? The objective is to develop a coupled thermal-structural finite element model (FEM) in ANSYS Workbench, validate the thermal predictions against published experimental results, and quantify the peak thermal stress, thermal strain, and total deformation together with their spatial localisation across the selected heat flux range. This approach provides a clearer basis for evaluating the thermomechanical suitability of 6061 aluminium alloy under the plasma loading conditions considered in this work.

2. Methodology

In industrial plasma applications especially cold plasmas (like: Plasma etching, surface modification, thin-film deposition), the electronic parameters (electron temperature, electron density) are vary widely depending on plasma process. These key parameters are the source of energy and outcome, which determining the energy flow within plasma systems and help in understanding energy transferring where controlling or measuring heat flux. In this research, a 3D model of specimen was firstly designed and then modelled using ANSYS Workbench 2020 R1 with the aim of visualizing the effect of altering the amount of heat plasma source values on the mechanical properties of 6061 Al Alloy for these applications [13]. This change in the values was initially resulting from the electron density, see Table 1. The numerical parametric study was then carried out in order to highlight some of the main mechanical properties such as the strength, the strain and the deformation. The experiments in Ref. [20] were conducted on a 3D printing RGD 525 specimen with the same geometry and boundary conditions used in the present model. The specimen was subjected to a controlled surface heating condition representative of the plasma heat input, and the surface temperature was imported to the specimen geometry in the structural analysis setting using (the coupled static-structural model with the purpose of determining the specimen's deformation). The heating duration and steady state condition were set, based on the plasma values, and the ambient conditions were fixed. These experimental measurements provide the reference temperature distribution and deformation values used for model validation. Validation was performed by comparing the numerical and experimental deformation at the same measurement location(s). The reported 4.4% corresponds to the relative error in the peak surface deformations.

In this work, the term plasma source refers to the thermal load delivered to the solid surface during low temperature argon plasma processing, where the dominant contribution to surface heating can be approximated by the electron energy flux reaching the wall. The objective is not to resolve a full plasma discharge or sheath in ANSYS, but to apply a bounded and physically plausible surface heat flux that represents the plasma surface interaction and then quantify the coupled thermal structural response of the Al6061 specimen.

Representative ranges of electron temperature and electron density were selected for low temperature RF argon plasmas used in surface modification and thin film processes. The electron temperature range is taken as T_e= 2 to 10 eV and the corresponding electron density is taken in the range ne approximately 10^{17} to 10^{18} m^{-3}. These ranges are consistent with partially ionized low temperature plasmas at sub atmospheric pressure. The values listed in table (1) are therefore used as representative cases for estimating the imposed surface heat flux applied in the subsequent ANSYS simulations, rather than as a complete characterization of a specific plasma device.

Table (1) Electronic plasma parameters (electron Temperature (Te), electron Density (ne), electron thermal velocity (vth)) and Heat Flux (q))

T_e (eV)	n_e (m^{-3})	v_{th} (m/s)	q (MW/m^2)
2	2.633×10^{18}	8.382×10^{5}	0.70687
4	9.314×10^{17}	1.185×10^{6}	0.70697
6	5.070×10^{17}	1.451×10^{6}	0.70683
8	3.293×10^{17}	1.673×10^{6}	0.70577
10	2.356×10^{17}	1.874×10^{6}	0.70551

Table (1) presents the electron temperature (T_e), the electron density (n_e), the electron thermal velocity (v_{th}), and the matching surface heat flux (q), given in SI units. The values of the electron thermal velocity (v_{th}), and the matching surface heat flux (q) are obtained from Eqs. (1) to (3), and a sample calculation is provided in Section 3 to allow reproducibility. Although the electron temperature (T_e) increases while ne decreases over the selected cases, their combined effect in the simplified formulation produces a limited variation in the matching surface heat flux (q). For this reason, the ANSYS parametric study treats the plasma loading primarily as a bounded representative uniform surface heat flux range (q = 0.5 to 0.7 MW/m^2) to evaluate the thermal structural response of Al6061 under conditions relevant to plasma surface processing.

3. Governing Equations and Analytical Method

To relate the plasma electron parameters to an equivalent thermal load on the solid, an order of magnitude estimate of the electron energy flux to the wall is used. The electrons are assumed Maxwellian, and the wall heat input is approximated by a free streaming electron energy flux formulation. Detailed sheath physics such as sheath potential drop, Bohm flux limits, secondary electron emission, and non-Maxwellian electron energy distributions are not explicitly resolved, because the present study focuses on the thermomechanical response of the solid under a representative plasma heat load rather than a detailed plasma discharge model [1,2,4]:

The surface heat flux associated with electrons impacting the wall is estimated from

$$q = n_e.(eT_e).v_{th} \quad \text{MW/m}^2 \quad (1)$$

where v_{th} is the thermal velocity of electrons (m/s), n_e is the electron number density (m^{-3}), and e is the elementary charge (C)

The ion heat flux to the wall is neglected in this study. At 1 Torr argon plasma, frequent ion neutral collisions lead to rapid energy exchange and effective cooling of ions, so ions tend to be close to the neutral gas temperature. In addition, the ion mean free path is short at this pressure, therefore ions reaching the near wall region are expected to carry limited thermal energy compared with electrons within the present simplified heat flux model.

The electron thermal velocity (m/s) is estimated as:

$$v_{th} = \sqrt[2]{\frac{2(eT_e)}{\pi m_e}} \quad (2)$$

where m_e is the electron mass

In this work, ne is taken from the temperature dependent relation adopted in Eq. (3) to generate the representative cases listed in table (1)

$$n_e \approx \frac{7.44\times10^{18}}{T_e^{\frac{3}{2}}} \quad (\text{m}^{-3}) \quad (3)$$

The resulting heat flux values in table (1) are obtained by substituting Eqs. (2) and (3) into Eq. (1). As the electron temperature (T_e) increases, the thermal velocity (v_{th}) increases too, while the electron number density (n_e) decreases across the selected cases, leading to a nearly constant matching surface heat flux (q) within the reported range. This behaviour reflects the chosen n_e-T_e coupling in Eq. (3) and the simplified electron energy flux formulation and it should be interpreted as a bounded representative heat flux for the subsequent FE study rather than as a universal plasma scaling.

The computed q values are implemented in ANSYS as a prescribed uniform surface heat flux boundary condition applied to the top surface of the specimen in the Steady State Thermal analysis. The resulting temperature field is then transferred to the Static Structural analysis to compute thermal stresses, strains, and deformations. No volumetric plasma heating inside the solid is applied, and radiation and convection losses are neglected to isolate the effect of the imposed plasma heat flux on the structural response.

In this study, Eqs. (1) to (3) are used to provide an order of magnitude estimate of the surface energy input for low temperature RF argon plasma processing. The plasma surface interaction is treated using a simplified free streaming electron energy flux approximation to relate electron temperature and electron density to a representative surface heat flux. A sheath limited model (for example Bohm flux), detailed sheath potential effects, and secondary electron emission are not explicitly resolved. The ion energy flux is neglected in the present formulation because the objective is to apply a bounded representative thermal load for the solid mechanics response rather than to develop a full plasma sheath energy balance. Radiative losses, surface recombination heating, and volumetric plasma heating inside the solid are not included. Consequently, the applied heat flux is treated as a prescribed uniform surface boundary condition in ANSYS, with the chosen range intended to be representative of the processing regime considered.

The stress fields result from the combined consequence of the dynamic stress, the vibratory stress and the thermal gradient. To compute the thermal stress, the following equation is employed [3,14,15]:

$$\sigma = \text{D}.\varepsilon \quad (4)$$

where σ, ε and D are stress, the strain and the matrix of elasticity, respectively

The considered material for the present study is the isotropic 6061 Al Alloy, table (2), and for the stress it's subjected to, it is within the elastic deformation range, thus, the relations of the stress–strain has been written in Cartesian coordinates such as the forms of equations (5-7) [10,16,17]:

The electron temperature (T_e) reported in table (1) is a plasma parameter used only to estimate the imposed surface heat flux, and it does not represent the temperature of the Al6061 specimen. In the present simulations, Al6061 properties in table (2) are treated

as constant because the structural response is evaluated based on the predicted solid temperature field. Implementing temperature dependent material properties for Al6061 is identified as an extension for cases where the computed solid temperatures become sufficiently high to significantly reduce stiffness.

Table (2) 6061 Al Alloy (Isotropic Elasticity)

Young's Modulus (MPa)	Poisson's Ratio	Bulk Modulus (MPa)	Shear Modulus (MPa)
2.83e+10	0.33	6.696e+10	2.56e+10

In the present simulations, Al6061 was modelled as an isotropic, linear elastic solid to quantify the first order thermoelastic response under the imposed plasma heat flux range. The material was implemented in ANSYS using the constant properties listed in table (2), that is temperature independent Young's modulus, Poisson's ratio, and coefficient of thermal expansion. Temperature dependent elastic modulus, thermal expansion, thermal conductivity, and yield strength were not implemented. Plastic deformation, creep, and microstructural anisotropy were therefore not included. This simplification is considered appropriate for the current loading range because the predicted stress levels are only on the order of a few MPa, approximately 4 to 6 MPa at the maximum applied plasma heat flux, which is significantly below the yield strength of Al6061, and the resulting deformations remain in the micrometre range. Hence, plasticity is not expected under the investigated conditions. Nevertheless, for cases involving higher heat fluxes, substantially higher surface temperatures, or long exposure times, plasticity and creep may become relevant and a thermo elastic-plastic model with tabulated temperature dependent properties should be adopted. Implementing such temperature dependent properties in ANSYS and validating them against experimental temperature and deformation measurements is identified as an important extension of the present work.

The plasma effect is represented in the thermal model as a prescribed surface heat flux boundary condition. The steady state temperature field obtained from the thermal analysis is then imported into the structural analysis. The resulting nonuniform temperature distribution produces thermal strain, which is converted to stress through the constitutive relation. Therefore, equations (5) to (7) are applied to relate the computed temperature change to thermal strain and the corresponding stress field, irrespective of whether the thermal load originates from plasma heating, laser heating, or any other surface heat flux source.

$$\varepsilon_x = \frac{1}{E}\left[\sigma_x - V_p(\sigma_y + \sigma_z)\right] + \alpha\Delta T(x,y,z) \quad (5)$$

$$\varepsilon_y = \frac{1}{E}\left[\sigma_y - V_p(\sigma_x + \sigma_z)\right] + \alpha\Delta T(x,y,z) \quad (6)$$

$$\varepsilon_z = \frac{1}{E}\left[\sigma_z - V_p(\sigma_x + \sigma_y)\right] + \alpha\Delta T(x,y,z) \quad (7)$$

where E is Young modulus, α is the coefficient of thermal expansion and V_p is the Poisson's ratio [1,11]

The temperature gradient, which is precisely bought from the CFD aerodynamic results, at points (x, y, z) is represented by ΔT(x, y, z). The numerical method is another significant way that is operated to provide fairly accurate results. Then, these results can be evaluated using some analytical and or experimental values in order to give conformity for them. Finite element analysis (FEA) is one of more than a few theories which gives numerical results for each; rigid radicalization and dynamic behaviour structures. However, it is considered one of the main utilized methods which lead to very accurate and reliable results [12,18]. In any numerical solution, specifically talking about the FEA; the first step, after selecting the material type, Fig. (1).

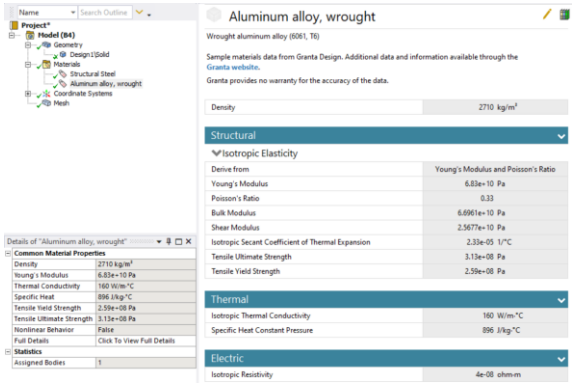

Fig. (1) Specifying the Al6061 alloy in ANSYS Workbench/ Material assignment [19]

Usually, selecting the element type which can be chosen based on the problem application and the geometry of the model (Fig. 2a), where the mechanical properties of the geometry or the structure under study can be found in any reference material books or brought experimentally. Subsequently, the values, the types and the directions of the applied loads should be specified, and the model problem can be solved based on the relevant chosen equations of solutions, (Fig. 2b). Element type is crucial. It should be chosen very carefully in order to accurately achieve the required solution. Accordingly, the element of (SOLID186) [19], was selected in the current work as it has six degrees of freedom as well as some other dynamic physical characteristics.

At this point, it is important highlight that not only the element type is important; the number of elements, which will make the mesh, is also a vital factor, where the large element size leads to low number of element and as a result to inaccurate results. On the other hand, the large number of elements will cost more time and effort without any actual benefit in terms of results' accuracy. So, the mesh sensitivity should be done in order to overcome this issue accurately (Fig. 3). Once that done; the load type, plasma flux, a small amount of

its pressure as well as their values and positions value can be applied, see the appendix, by doing that, the model will be ready to be solved by using the governed equations.

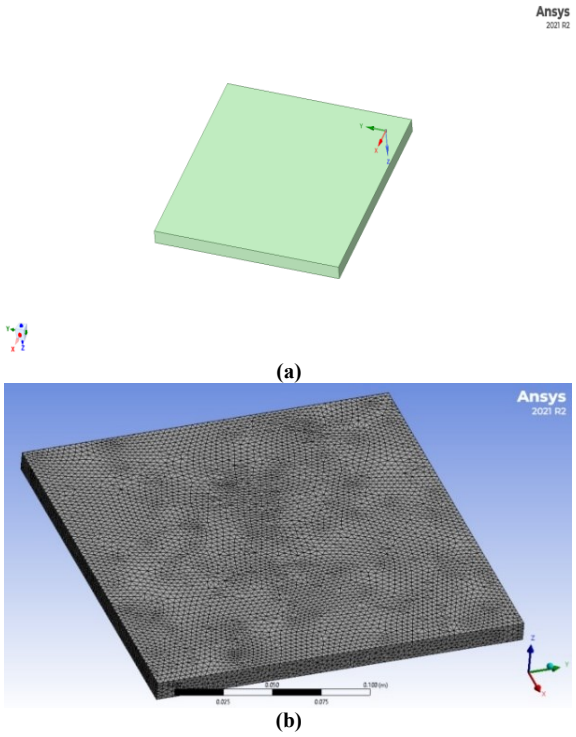

Fig. (2) Designing and generating the model geometry using ANSYS SpaceClaim (a) and structural mesh using the assigned element type of the refined mesh of the model (b) [12]

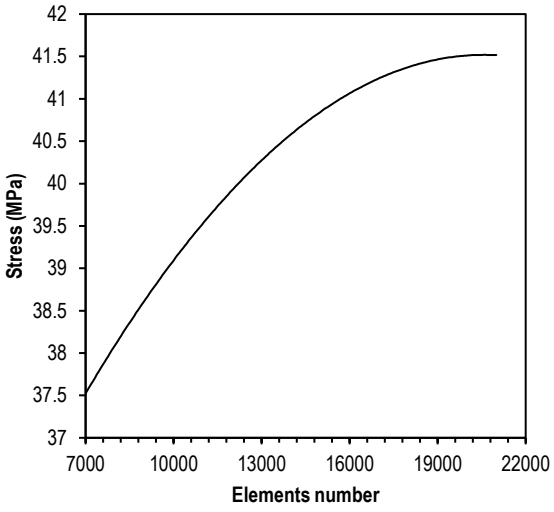

Fig. (3) Mesh sensitivity to correctly choose the required number of the assigned element

3.1 Numerical Model Setup and Solver Settings

3.1.1 Geometry and Dimensions

The specimen was modelled as a 3D solid in ANSYS SpaceClaim. The geometry corresponds to a rectangular plate specimen and the dimensions used in the model are length (L) of 200 mm, width (W) of 200 mm, and thickness (t) of 10 mm. The top surface (z = t) represents the plasma exposed face.

3.1.2 Thermal Boundary Conditions

A Steady State Thermal analysis was performed. A uniform surface heat flux (q) in the range 0.5 to 0.7 MW/m^2 was applied to the top surface to represent plasma heating. The remaining external surfaces were treated as adiabatic. Convection and radiation were neglected in order to isolate the effect of the imposed plasma heat flux on the temperature field used for the coupled structural response.

3.1.3 Structural Boundary Conditions and Coupling

The thermal solution was imported into a Static Structural analysis. The bottom surface (z = 0) was constrained using a fixed support (all translational degrees of freedom constrained), while the remaining faces and edges were left free to expand. This configuration allows thermal expansion driven deformation while preventing rigid body motion. The material model for Al6061 was assumed isotropic and linear elastic using the properties listed in table (2).

3.1.4 Mesh and Mesh Independence

The solid geometry was meshed in ANSYS Mechanical using the built-in meshing module. A mesh sensitivity study was carried out by progressively refining the global element size and monitoring the resulting von Mises stress. As shown in Fig. (3), the stress increases with mesh refinement and then approaches a plateau, with only marginal changes beyond approximately 18000 to 20000 elements. Based on this convergence behaviour, a mesh of about 20000 elements was selected for all subsequent simulations to ensure mesh independent results while maintaining reasonable computational cost.

3.1.5 Solver Settings

The Steady State Thermal solver used default convergence tolerances in ANSYS Workbench 2020 R1. The Static Structural analysis was solved using the imported temperature field and linear elastic formulation. Large deformation effects were enabled and the stress results reported correspond to the converged solution for each applied heat flux case.

Boundary conditions were defined as follows. Thermally, a uniform heat flux (q) of 0.5-0.7 MW/m^2 was applied to the top surface to represent the plasma heating. The remaining external surfaces were modelled as thermally insulated, and heat losses by convection and radiation were not included in order to isolate the influence of the imposed plasma heat flux within the coupled thermal structural analysis. Mechanically, the bottom surface of the specimen was modelled with a fixed support (all translational degrees

of freedom constrained), while the other faces and edges were left free.

As a consequence, the achieved results should be assessed by comparing them with some experimental or analytical results in order to make sure that the applied steps were accurately selected and performed.

In this paper, the mentioned results referred to the stress, strain, deflection and the fatigue analysis. Figure (4) shows the mentioned steps in terms of a flow chart.

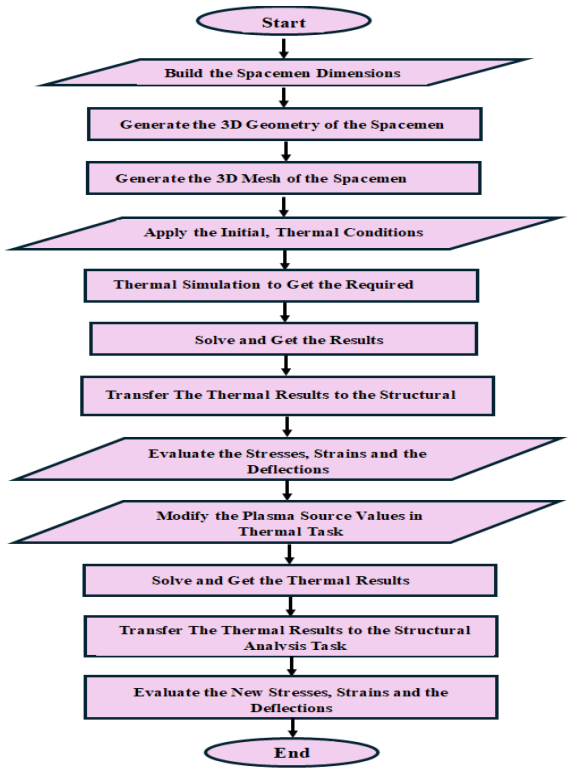

Fig. (4) Overview process of the analysis procedures followed for the current simulation

6. Results and Discussions

In low-density or collision-less plasmas, such as those in space, heat flux is dominated by free-streaming electrons rather than collisional conductivity. To enable quantitative comparison between cases, the following metrics are reported for each applied plasma heat flux: maximum temperature on the exposed surface, maximum through thickness temperature gradient, maximum von Mises stress, maximum equivalent elastic strain, and maximum total deformation. These values are used to evaluate sensitivity to heat flux and to benchmark the predicted stresses and strains against the mechanical limits of Al6061.

In low-density or collision-less plasmas, such as those in space, heat flux is dominated by free-streaming electrons rather than collisional conductivity. The heat flux in plasma generally follows a relationship of electron temperature and plasmas densities and its rises due to temperature gradients, particle motion and its collisions, which describes the rate of energy transition through area in the plasma. Physically as the electron number density (n_e) increases or decreases, resulting in a lower heat flux, this is done because collisions are more frequent in high-density plasmas, which inhibits the free flow of heat-carrying electron. A steep gradient in electron temperature (T_e) differences over short distances drives a large heat flux, as more energy is transferred across the plasma boundary but the inverse relation between electron number density (n_e) and electron temperature (T_e) made-balance in heat flux (q) values. Controlling the electron temperature (T_e) and electron number density (n_e) ensures targeted heat flux and deformation effects on aluminum alloys, making plasma a versatile tool for both bulk and surface modifications. As the electron temperature (T_e) increases, the energy carried by each electron increases, leading to a higher heat flux. This is because hotter electrons have more kinetic energy and thus can transfer more heat. As the electron number density (n_e) increases, the number of electrons available to transfer heat also increases, which raises the heat flux proportionally.

In this work, a FEA of 3D Al6061 alloy model was numerically simulated with the aim of finding out the effect of plasma as a heat source on its mechanical properties of the material. First of all, the numerical model was initiated for an experimental result for Al6061 alloy found in the literature in order to make sure that the followed procedure was correct. Once the differences between the results of the two models were within the allowed limit, the analyses were accordingly carried out, prepared, presented and discussed as follows.

The numerical analyses were carried out with the aim of highlighting the effect of varying the plasma flux values on the above-mentioned outlet parameters. This requires coupling both the static structural analysis with the thermal analysis in the ANSYS Workbench tasks (Fig. 5). Once the solution completed, the von Mises stress, normal stress, von Mises strain, thermal elastic strain, directional deformation and the total deformation for the Alloy model at the highest and lowest applied plasma source value are figured out.

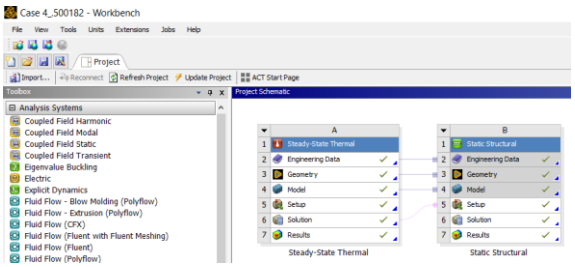

Fig. (5) The coupled thermal analysis and static structural analysis in ANSYS Workbench tasks

Figure (6) shows the von Mises stress contours at the model geometry at plasma source values of 0.5

MW/m^2 and 0.7 MW/m^2 (LHS & RHS) respectively. In this figure, it is clear that by fixing all other boundary conditions (BCs) and only increasing the flux value on the specimen, a small amount of stress concentration will be noticed on the specimen corners for both cases. This, however, occurred in an undistributed manner, moreover, with a high, relatively, value. For example, maximum stress values of about 4.3 MPa and 5.9 MPa were shown at the mentioned areas of the specimen to represent each; the von Mises stress at maximum and minimum applied plasma flux values, respectively. Furthermore, most of the specimen was coloured with the yellow to red colour to highlight the fact that a large part of its body was affected with the applied plasma flux load. This, in fact, gives a good indication about the alloy's ability to withstand like these loads during the real applications, as the stress was uniformly distributed on the all-specimen body except the areas in red colour, i.e., the specimen's four corners.

The plasma heat load is applied as a uniform surface heat flux on the top surface of the specimen. The thermal analysis is performed under steady state conditions, as shown in Fig. (6). Convection and radiation heat losses are not included in this study. The bottom surface thermal condition is defined as fixed temperature, while the bottom surface is mechanically constrained in the structural analysis. The plasma pressure effect was not included in this study.

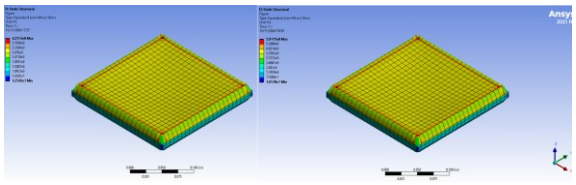

Fig. (6) von Mises stress distribution upon the specimen body at the minimum (LHS) and maximum (RHS) applied plasma values

In the same manner, figure (7) shows the normal stress contours at the model geometry at (LHS & RHS) respectively. In this figure, it is clear that by fixing all other boundary conditions (BCs) and only increasing the flux value on the specimen, no real stress concentration will be noticed on the specimen's body at each, the lowest and highest plasma values. It is shown that the maximum stress values were about 1.5 MPa and 2.6 MPa at the mentioned areas of the specimen at maximum and minimum applied plasma flux values, respectively. Moreover, the all specimen was coloured with the green colour to highlight the fact that all the specimen body was affected with the applied plasma flux load. Again, this is another proof on the alloy's ability to withstand like these loads during the real applications, as the stress was uniformly distributed on the all-specimen body except the areas in red colour i.e., the specimen four corners.

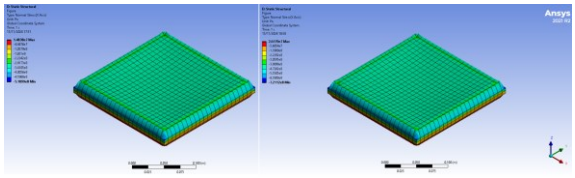

Fig. (7) Normal stress distribution upon the specimen body at the minimum (LHS) and maximum (RHS) applied plasma values

Figure (8) provides a comprehensive visual representation of the von Mises strain contours corresponding to the specific model geometry under the influence of plasma source values denoted as 0.5 MW/m^2, and 0.7 MW/m^2 (LHS & RHS), respectively. Within the confines of this figure, it becomes abundantly evident that when all other boundary conditions (BCs) are held constant and the flux value applied to the specimen is incrementally increased, there will be a discernible yet minor concentration of stress manifesting at the corners of the specimen for both scenarios examined. Nevertheless, it is crucial to note that this occurrence transpires in a manner that is not uniformly distributed across the specimen, and significantly, the strain values recorded are relatively elevated. In addition, a substantial portion of the specimen's surface was depicted in a gradient of yellow to red hues, serving to emphasize the reality that a considerable segment of its structural integrity was impacted by the imposition of the plasma flux load. This observation, in fact, offers a significant insight into the alloy's capacity to endure such load conditions during practical applications, as the strain was largely homogeneously distributed throughout the entirety of the specimen's body, with the notable exception of the areas highlighted in red, specifically the four corners of the specimen where stress concentrations were most pronounced.

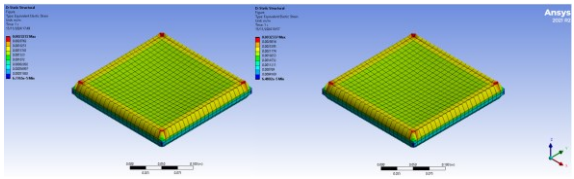

Fig. (8) von Mises strain distribution upon the specimen body at the minimum (LHS) and maximum (RHS) applied plasma values

Figure (9) shows the equivalent elastic strain contours for the specimen subjected to plasma heat flux values of 0.5 MW/m^2 and 0.7 MW/m^2. With the boundary conditions kept constant, increasing the applied heat flux leads to a small increase in the strain magnitude, with localized peaks appearing at the specimen corners, where the constraint and geometric discontinuities promote strain concentration. Importantly, the corrected strain values are not elevated as previously reported. The maximum equivalent elastic strain is on the order of 10^{-3}, reaching about

0.0023 m/m, while the minimum values are on the order of 10^{-5} m/m. The strain field remains largely uniform across the central region of the specimen, with a clear through thickness gradient, which is consistent with thermally induced deformation caused by the imposed temperature gradient. Overall, the results indicate an elastic response under the investigated heat flux range, with localized strain concentration limited to the corner regions.

Also, the total deformation of the specimen's model is given in the current study, see Fig. (10), because of its vital importance. It is clear from the given contour that the top side of the specimen had the maximum values of the deformation, especially at the specimen centre in both cases. However, the deformation at the minimum plasma flux value applied, which is around 8.6 µm, differs from that at the maximum plasma flux value, i.e., 12 µm. At this point, it should be mentioned that in both cases, the specimen has not experienced any deformation at the bottom side of the specimen. This is also another good mark, especially when most of the model was suffering from the deformation without having a plastic deformation at a specific part of the geometry.

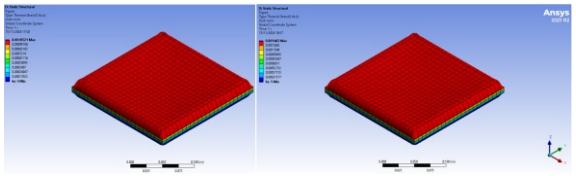

Fig. (9) Thermal strain contour on the specimen body at the minimum (LHS) and maximum (RHS) applied plasma values

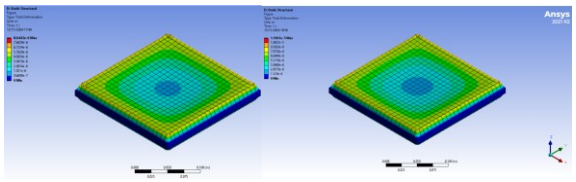

Fig. (10) Total deformation contour on the specimen body at the minimum (LHS) and maximum (RHS) applied plasma values

Furthermore, figure (11) gives the directional deformation (in x-axis) as it was the only direction that showed a response to the applied plasma. It is imperative to note that the comprehensive measurement of the total deformation experienced by the specimen's model is meticulously presented in the current research endeavour, due to its considerable significance in understanding the behaviour of the material under investigation. Upon careful examination of the provided contour plots, it becomes evident that the uppermost region of the specimen exhibited the highest recorded values of deformation, with particular emphasis on the side portion of the specimen in both experimental scenarios evaluated to show both; the maximum and the minimum deformation vales. Nevertheless, it is noteworthy that the deformation observed at the minimum plasma flux value of approximately 1.1 µm is distinctly different from that recorded at the other maximum plasma flux value, which measures around 15 µm. At this juncture, it is essential to highlight that in both experimental cases analysed, the specimen did not undergo any measurable deformation at the lower side, which is a significant finding; this observation is particularly commendable given that a substantial portion of the model exhibited considerable deformation while simultaneously maintaining the integrity of a specific section of the geometry without succumbing to plastic deformation.

Next, the maximum, the minimum, and the average values of each von Mises stress, normal stress, von Mises strain, thermal elastic strain, directional deformation, and the total deformation at all of the plasma source values have been figured out in figures (12), (13), and (14) respectively. Starting from Fig. (12a), it can be noticed that the range of the maximum von Mises stress values is relatively high compared to the minimum ones, especially at high plasma sources. This can be considered a good sign as there are no inversion stresses that affect the specimen, which lead to a fast deterioration in the specimen geometry and a failure. A similar trend is noticed in the values of normal stresses; however, with a higher amount of minimum stresses at all the applied plasma values, given in Fig. (12b). This also increases the level of current results' accuracy.

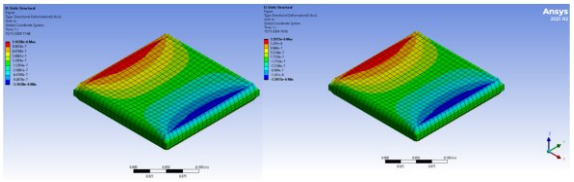

Fig. (11) Directional deformation contour on the specimen body at the minimum (LHS) and maximum (RHS) applied plasma values

Across the investigated heat flux range, the maximum von Mises stress increases from approximately 425 MPa to 591 MPa, while the maximum equivalent elastic strain increases from $7.61\text{x}10^{-4}$ to $5.56\text{x}10^{-4}$. The peak stresses are located near the constrained region, where thermal expansion is restricted and the temperature gradient induces bending. Importantly, the maximum stress remains only on the order of a few MPa (about 4 to 6 MPa at the maximum heat flux), which is well below the yield strength of Al6061. This indicates that the response remains in the elastic regime for the conditions considered. For higher heat fluxes or longer exposures leading to higher temperatures, temperature dependent properties and elasto-plasticity should be included to assess yield onset and permanent deformation.

The next two figures, i.e., figures (13a) and (13b), showed the von Mises, equivalent strain and thermal strain changing trend with respect to the variation of plasma source values. Again, very similar trends have been shown in both figures.

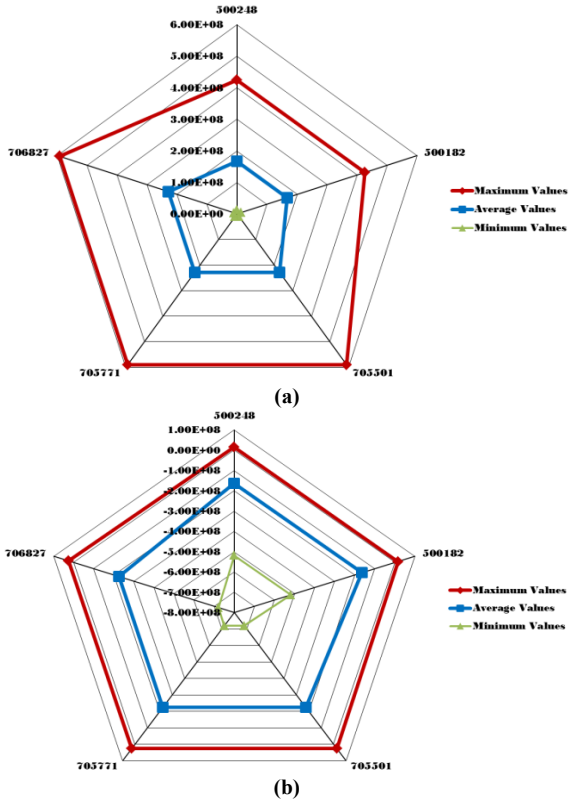

Fig. (12) von Mises (a) and Normal stress (b) on the specimen body at various applied plasma values

At the highest applied heat flux, the minimum strain values become negative in localized regions. This indicates a change in strain sign (compressive thermal strain) caused by the nonuniform temperature field and constraint conditions, where some parts of the specimen expand while others experience restrained contraction. This behaviour is not indicative of buckling or plasticity, since the predicted stresses remain on the order of a few MPa and the deformations are in the micrometre range within the linear elastic regime. No buckling instability was modelled in this study because the structural analysis is linear and the deformation remains small.

The subsequent two graphical representations, given in figures (14a) and (14b) presented in this analysis depict the intricate variations of the von Mises equivalent strain alongside the thermal strain as they correlate to the fluctuations observed in the plasma source parameters, thereby providing a comprehensive understanding of their interdependencies. Additionally, it is noted that both figures exhibit remarkably analogous trends, reinforcing the consistency of the observed phenomena across the different graphical representations. Having said that, it also should be mentioned that the lowest strain values, which were recorded to be at the location of maximum plasma intensity, highlights an anomalous inverse direction of the strain; this observation serves as a concerning indicator regarding the structural integrity and resilience of the model currently under scrutiny, specifically in the context of elevated flux conditions.

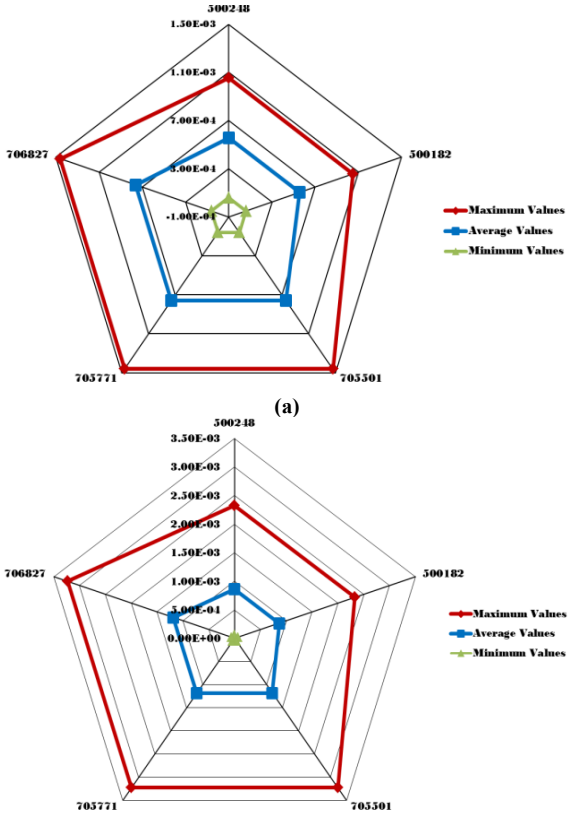

Fig. (13) von Mises strain (a) and Thermal Strain (b) on the specimen body at various applied plasma values

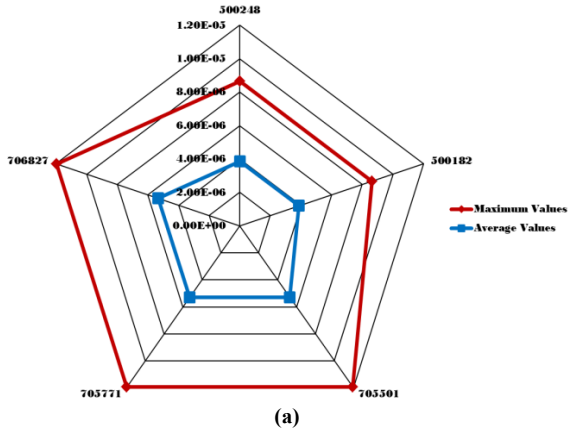

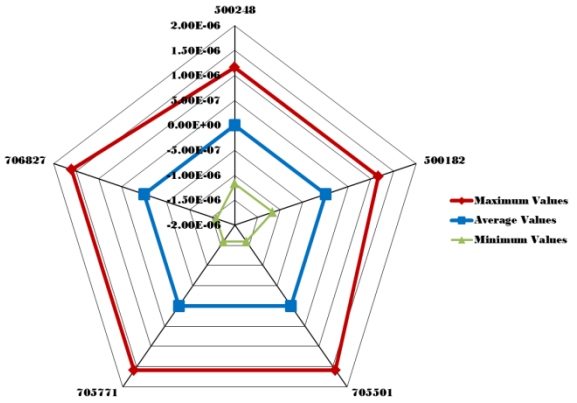

(b)

Fig. (14) Total deformation (a) and Directional deformation (b) on the specimen body at various applied plasma values

7. Conclusions

The effect of plasma source heat flux on the thermal and structural response of 6061 Al alloy was evaluated in this work using 3D FEA across a range of plasma parameters (electron temperature: 2-10 eV, electron density: 2.356×10^{17} to 2.633×10^{18} m^{-3}, heat flux: 0.70551-0.70697 MW/m²). Based on the numerical analysis, the following specific observations were made. At the maximum applied plasma heat flux (0.707 MW/m²), the von Mises stress reached approximately 5.9 MPa, representing only 27% of the material's yield strength (assumed based on typical 6061 Al alloy properties). The stress was uniformly distributed across the specimen body, with minor concentrations (4.3-5.9 MPa) observed only at the four corners. The maximum von Mises strain at peak plasma flux was approximately 2.6×10^{-4}, which is well within the elastic deformation range for this alloy. Thermal strain values ranged from $1.0\text{-}1.5\times10^{-4}$ across the specimen. Total deformation at maximum plasma flux was 12 µm (directional deformation: 15 µm in x-axis), confined primarily to the top surface and centre of the specimen, with no measurable deformation at the bottom surface. This indicates that the deformation remained within elastic limits. The edges and corners of the specimen geometry consistently exhibited the highest stress and strain concentrations across all plasma flux values tested, identifying these as potential failure initiation sites that require consideration in component design.

Acknowledgment

The authors would like to thank the University of Mosul for the facilities provided for this study.

References

[1] M.A. Lieberman and A.J. Lichtenberg, "Principles of plasma discharges and materials processing", *MRS Bull.,* 30(12) (1994) 899-901.

[2] Y. Ueda et al., "Baseline high heat flux and plasma facing materials for fusion", *Nucl. Fusion*, 57(9) (2017) 092006.

[3] N.E. Dowling, **"Mechanical Behavior of Materials: Engineering Methods for Deformation, Fracture, and Fatigue"**, 2nd ed., Prentice Hall (1999).

[4] A. Maksimov and V. Silin, "Heat-flux limitation factor in a plasma", *Soviet J. Exper. Theor. Phys. Lett.*, 58 (1993) 271.

[5] N. Saruwatari, H. Kagami and Y. Nakayama, "Effect of short-time heating after ECAP processing on mechanical properties of 6061 aluminum alloy", *Mater. Trans.*, 64(2) (2023) 429-35.

[6] G. Wang et al., "Effect of heat treatment conditions on mechanical properties and springback of 6061 Aluminum alloy sheets", *IOP Conf. Ser.: Mater. Sci. Eng.,* 788 (2020) 012056.

[7] J. Wang et al., "Effect of preheat & post-weld heat treatment on the microstructure and mechanical properties of 6061-T6 aluminum alloy welded sheets", *Mater. Sci. Eng. A*, 841 (2022) 143081.

[8] M. Kumar et al., "Effect of artificial aging temperature on mechanical properties of 6061 aluminum alloy", *Mehran Univ. Res. J. Eng. Technol.*, 38(1) (2019) 31-36.

[9] Ł. Wzorek et al., "Effect of heat treatment on quality and properties of solid bonded 6061 aluminum alloy", *Inżynieria Materiałowa*, 38(1) (2017) 104143.

[10] D. Maisonnette et al., "Effects of heat treatments on the microstructure and mechanical properties of a 6061 aluminium alloy", *Mater. Sci. Eng. A*, 528(6) (2011) 2718-2724.

[11] K.L. Lawrence, ANSYS workbench tutorial release 14. SDC publications (2012).

[12] T. Stolarski, Y. Nakasone and S. Yoshimoto, **"Engineering analysis with ANSYS software"**, Butterworth-Heinemann (2018).

[13] M. Scapin and A. Manes, "Behaviour of Al6061-T6 alloy at different temperatures and strain-rates: experimental characterization and material modelling", *Mater. Sci. Eng. A*, 734 (2018) 318-328.

[14] A.M. Daabo et al., "A Novel Design of a Hybrid Micro-Scale Multistage Turbine Model for Sustainable Energy Sources", *Case Stud. Therm. Eng.*, 74 (2025) 106873.

[15] J. Lemay, "Modal analysis of power system dynamics", PhD thesis, McGill University, Canada (1972).

[16] K. Chanyathunyaroj et al., "Fatigue characteristics of 6061 aluminum alloy subject to 3.5% NaCl environment", *Int. J. Fatigue*, 133 (2020) 105420.

[17] A.M. Daabo, S. Mahmoud and R.K. Al-Dadah, "Structural analysis of small scale radial turbine for solar powered Brayton cycle Application", *Energy Sustain.,* 51418 (2018) V001T11A10.

[18] A.M. Daabo et al., "Parametric study of efficient small-scale axial and radial turbines for solar powered Brayton cycle application", *Ener. Conver. Manage.*, 128 (2016) 343-360.
[19] ANSYS CFX-Solver Theory Guide, ANSYS, Inc. (USA), Release 12.1, November 2009.
[20] A.M. Daabo et al., "Experimental study and 3D optimization of small-scale solar-powered radial turbine using 3D Printing technology", *Machines,* 11(8) (2023) 817.

Appendix I: Applied load on the designed model.

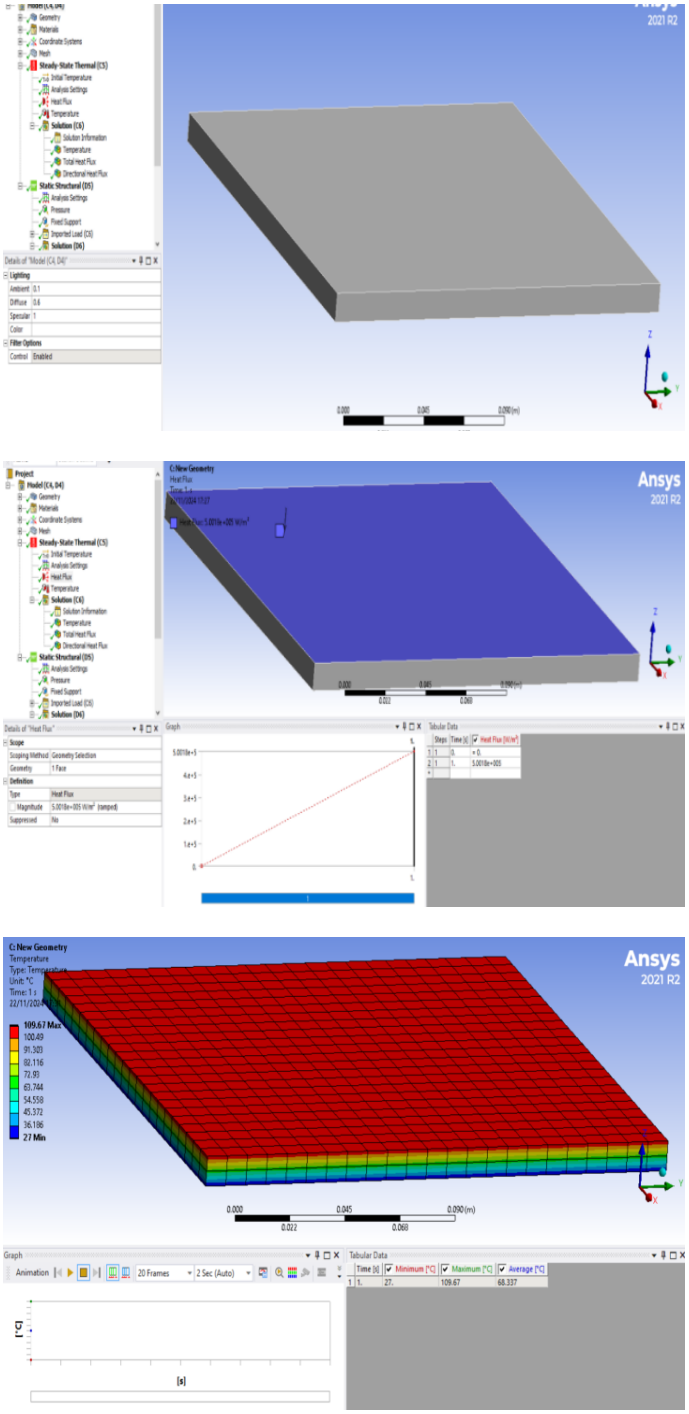

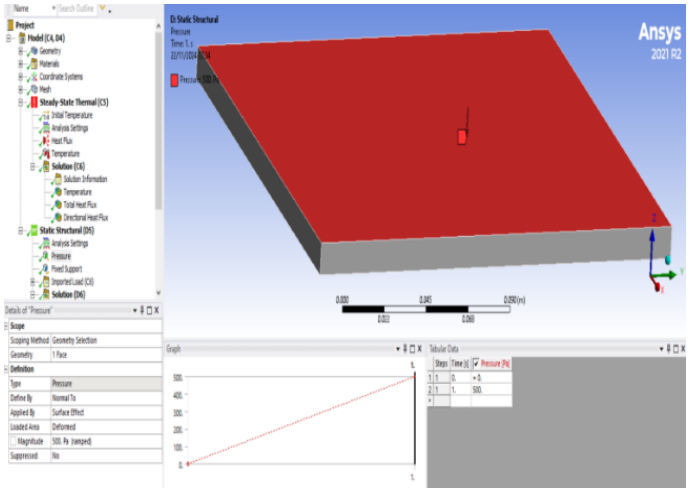
Ansys
2021 R2

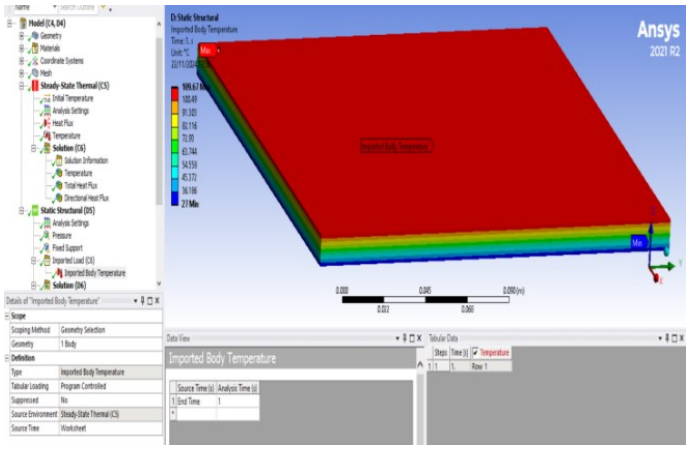
Ansys
2021 R2
Imported Body Temperature

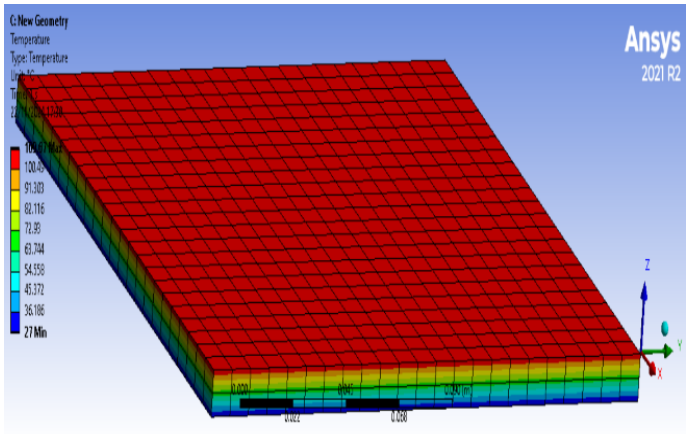
Ansys
2021 R2
C:New Geometry
Temperature
Type: Temperature
27 Min